Rare-Earth-Less Motor with Field Poles Excited by Space Harmonics

— Theory of Self-Excitation and Magnetic Circuit Design —

Masahiro Aoyama
Department of Environment and Energy System,
Graduate School of Science and Technology,
Shizuoka University
3-5-1 Johoku, Naka-Ku, Hamamatsu,
Shizuoka 432-8561, Japan
Electric Drive Vehicle Design Department
Suzuki Motor Corporation
aoyamam@hhq.suzuki.co.jp

Toshihiko Noguchi
Department of Electrical and Electronic Engineering,
Graduate School of Engineering,
Shizuoka University
3-5-1 Johoku, Naka-Ku, Hamamatsu,
Shizuoka 432-8561, Japan
ttnogut@ipc.shizuoka.ac.jp

***Abstract*— This paper describes a synchronous motor in which space harmonics power is utilized for field magnetization instead of permanent magnets. The stator has a concentrated winding structure, and the rotor has two sorts of windings, i.e., an induction pole (I-pole) winding that retrieves mainly the third space harmonics and an excitation pole (E-pole) winding for the field magnetization. The both coils are connected via a diode rectifying circuit. By utilizing the E-pole torque magnetized with self-excitation, permanent magnet volume of the proposed motor is reduced by 81.4 %, compared with the benchmark IPM motor.**

Keywords—component; synchronous motor, self-excitation, induced current, field current, electromagnets

I. INTRODUCTION

In recent years, hybrid vehicles (HEVs) and electric vehicles (EVs) driven by shared power with an internal-combustion engine or only by electric power are focused on because of environmental concerns such as global warming, exhaustion of fossil fuels, and air pollution problems. An electric machine is one of the key parts in the HEVs and the EVs from the viewpoint of dynamic and fuel consumption performances. Traction motors for the HEVs have significantly unique features, compared with industry applied motors. Wide adjustable speed drive range, high maximum torque, high power density without sacrificing its efficiency are demanded to improve the total system efficiency. An IPM (Interior Permanent Magnet) motor is applied to the HEVs owing to its highly improved efficiency and specific power per physical volume. Permanent magnets used for the IPM motor are very expensive because Nd-Fe-B magnets are generally adopted to realize high energy density and to improve fuel efficiency at low load operation for street use. Moreover, the traction motors are usually installed on the chassis where special countermeasures must be taken for environmental and thermal issues. In order to restrain demagnetization caused by temperature rise of the permanent magnets for example, extremely expensive rare-earth metals such as Dy and Tb must be added to the Nd-Fe-B magnet.

A variety of rare-earth-less and rare-earth-free motors are recently proposed due to remarkable rise of Nd-Fe-B magnet market prices and a global maldistribution problem of the magnet material such as Dy and Tb. Wound-field motors that replace the permanent magnets with electromagnets are intensively investigated both in industries and in academia as post IPM motors [1][2]. For example, a separate excitation wound-field synchronous motor is proposed in [1]. This motor is capable to utilize armature reaction torque by wound-field torque, and the field magnetization control allows high efficiency operation. An external chopper circuit is, however, indispensable for the wound-field winding. Furthermore, it is rather difficult to transfer the field magnetization power from the primary to the secondary, and an extra copper loss in the wound-field winding is also a serious problem. Therefore, a self-excitation technique proposed in [3][4] is reevaluated by the authors to solve the problems regarding the separate excitation wound-field motors. The classic self-excitation based synchronous motor has a stator with distributed windings and a salient pole rotor with a single winding connected via a half-bridge rectifier. The second space harmonics linking to the rotor winding is utilized for the field magnetization. However, low linkage of the space harmonics to the rotor winding makes it difficult to improve the motor efficiency further. In addition, it is rather difficult to retrieve the space harmonics power because the single rotor winding plays both roles of an induction coil and an electromagnet coil at the same time.

In this paper, the problems of the classical self-excited synchronous motor are solved, and a new configuration and a new operation mechanism of the self-excitation are proposed, focusing on the space harmonics power of the motor. In general, the self-excited motors do not have sufficient field-magnetization power in the low speed range due to low

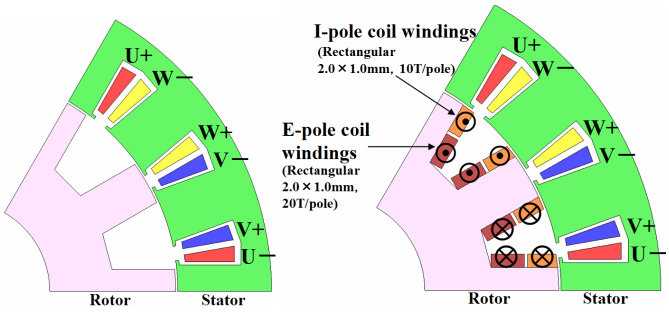

(a) SynRM. (b) Model 1 (without sub-poles).

Fig. 1. Cross section diagram of SynRM and model 1.

TABLE I SPECIFICATION OF MOTOR.

Number of poles	12
Number of slots	18
Stator outer diameter	200 mm
Rotor diameter	138.6 mm
Axial length of core	54 mm
Air gap length	0.7 mm
Maximum current	273 A_{pk}
Stator winding resistance	32.1 mΩ / phase
Number of coil-turn	48
Winding connection	6 parallel
I-pole winding resistance	12.1 mΩ / pole
E-pole winding resistance	26.9 mΩ / pole
Thickness of core steel plate	0.35 mm

induced voltage in the rotor winding, so a hybrid field magnetization of less rare-earth magnet and self-excitation type wound-filed to reinforce the field magnetization regardless of the operation speed is also discussed.

II. BRUSHING UP OF THE SELF-EXCITATION TECHNOLOGY

A. Full-Bridge Rectifiier and Double Rotor Windings

Figure 1(a) shows a SynRM (Synchronous Reluctance Motor) with a concentrated winding structure in the stator. Figure 1 (b) shows a motor (Model 1) where the wound-field coils are added to the rotor salient poles of the normal SynRM. Conventional common motors dissipate space harmonics power caused by the stator with the concentrated structure, whereas the proposed motor positively utilizes the space harmonics power for the field magnetization. Each of I-pole is a special pole exclusively used for the magnetizing energy generation from the third space harmonics. On the other hand, each E-pole is a salient pole on the rotor for the field excitation, which uses the retrieved third space harmonics power. Every I-pole and E-pole is connected in series via a diode rectifying circuit as shown in Fig. 2, where p means a pole number. Specifications of the motor shown in Fig. 1 are listed in Table I. Figure 3 shows output torque characteristics at 1000 r/min and

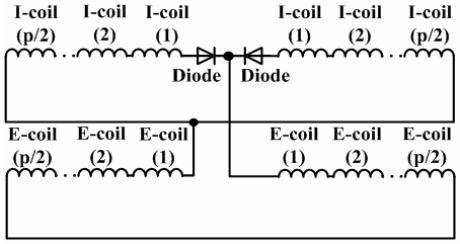

Fig. 2. Rotor winding connection diagram of full-bridge rectifier.

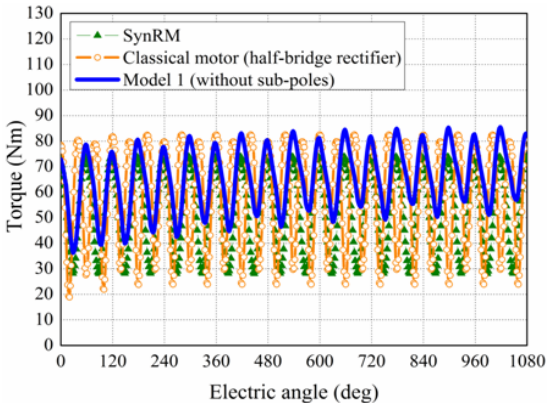

Fig. 3. Torque characteristics at 1000 r/min and 273A_{pk}.

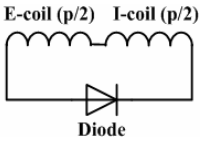

Fig. 4. Classical rotor winding connection diagram.

273 A_{pk} under MTPA (Maximum Torque Per Ampere) control calculated by an FEM based magnetic field analysis. As shown in Fig. 3, increase of the torque of Model 1 can be confirmed in comparison with the conventional SynRM shown in Fig. 1(a) and the classic self-excited motor that has a simple winding construction as shown in Fig. 4. This is because Model 1 can add the E-coil torque generated by the self-excitation to the conventional reluctance torque.

B. Sub-Poles in Space Harmonics Magnetic Path

Assuming a combination between the rotor pole counts and the stator slot counts is 2 to 3, a U-phase self inductance L_u can be given as

$$L_U(\theta) = L_{S0} + L_S \cos 2\theta \,, \tag{1}$$

where L_{S0} is a constant part and L_S is an amplitude of the periodical variation of the self inductance.

Hence, U-phase magnetic flux $\varphi_{S\text{-}U}$ is derived as

$$\phi_{S-U} = \frac{L_U(\theta) I_U(t)}{N_S} = \frac{\{L_{S0} + L_S \cos 2\theta\} I_S \cos(\omega t + \beta)}{N_S} \,, \tag{2}$$

where $I_U(t)$ is a U-phase armature current, N_S is the number of armature winding turn, and β is a current phase. Similarly, V-

phase magnetic flux $\varphi_{S\text{-}V}$ and W-phase magnetic flux $\varphi_{S\text{-}W}$ can be given as

$$\phi_{S-V} = \frac{\left\{L_{S0} + L_S \cos\left(2\theta - \frac{2}{3}\pi\right)\right\} I_S \cos\left(\omega t + \beta - \frac{2}{3}\pi\right)}{N_S}, \text{ and} \quad (3)$$

$$\phi_{S-W} = \frac{\left\{L_{S0} + L_S \cos\left(2\theta + \frac{2}{3}\pi\right)\right\} I_S \cos\left(\omega t + \beta + \frac{2}{3}\pi\right)}{N_S}. \quad (4)$$

Therefore, a three-phase armature flux is calculated as follows:

$$\phi_{S-UVW} = \phi_{S-U} + \phi_{S-V} + \phi_{S-W} = \frac{3}{2}\frac{1}{N_S} L_S I_S \cos(\omega t + \beta - 2\theta). \quad (5)$$

An α-axis magnetic flux $\varphi_{S\text{-}\alpha}$ and a β-axis magnetic flux $\varphi_{S\text{-}\beta}$ on the stationary orthogonal reference frame are obtained that converted two-phase static coordinates from three-phase static coordinates are given as:

$$\phi_{S-\alpha} = \phi_{S-U} + \phi_{S-V}\cos\frac{2}{3}\pi + \phi_{S-W}\cos\frac{4}{3}\pi$$
$$= \frac{I_S}{N_S}\left[\frac{1}{2}L_{S0}\left\{3\cos(\omega t + \beta) + \sqrt{3}\sin(\omega t + \beta)\right\} - \frac{1}{4}L_S\cos(\omega t + \beta - 2\theta)\right], \quad (6)$$

and

$$\phi_{S-\beta} = \phi_{S-V}\sin\frac{2}{3}\pi + \phi_{S-W}\sin\frac{4}{3}\pi$$
$$= \frac{3}{2}\frac{I_S}{N_S}\left[L_{S0}\sin(\omega t + \beta) + \frac{1}{2}L_S\sin(\omega t + \beta + 2\theta)\right]. \quad (7)$$

Applying a rotational coordinate transform to the above equation by using a d-axis phase θ_d and a q-axis phase θ_q expressed in Eq. (8), a d-axis magnetic flux $\varphi_{S\text{-}d}$ and a q-axis magnetic flux $\varphi_{S\text{-}q}$ can be obtained as Eqs. (9) and (10).

$$\theta_d = \omega t, \ \theta_q = \omega t - \frac{\pi}{2}, \quad (8)$$

$$\phi_{S-d} = \frac{I_{Sd}}{N_S}\left[\frac{1}{2}L_{S0}\left\{3\cos(\omega t + \beta) + \sqrt{3}\sin(\omega t + \beta)\right\} - \frac{1}{4}L_S\cos(-\omega t + \beta)\right],$$

and (9)

$$\phi_{S-q} = \frac{3}{2}\frac{I_{Sq}}{N_S}\left[L_{S0}\sin(\omega t + \beta) + \frac{1}{2}L_S\sin(3\omega t + \beta)\right]. \quad (10)$$

Figure 5 depicts relationship among the reference frames and a simplified model of the wound-field salient pole motor. As can be seen in the figure, the rotor salient pole is aligned with the d-axis and the q-axis is supposed to be between the two salient poles. An induced voltage in the rotor winding is caused by the magnetic flux linkages of the d-axis and the q-axis as expressed on Eqs. (9) and (10). For simplification of the calculation, a cross-linkage magnetic flux and a leakage magnetic flux are ignored. Since the dq reference frame rotates synchronously at the speed of an angular frequency ω, the rotor winding and the d-axis and the q-axis magnetic fluxes cause magnetic coupling of the frequency that is higher than the synchronous speed. Therefore, Eqs. (9) and (10) show that the space harmonics magnetic path is established on the q-axis. In addition, Eq. (10) shows that the field magnetization energy for the self-excitation is mainly obtained from the third space harmonics.

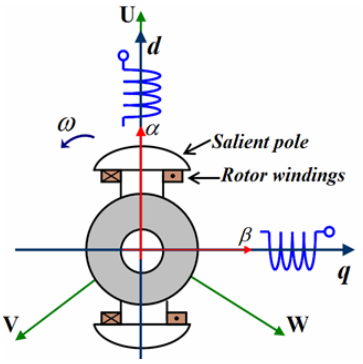

Fig. 5. Wound-field salient pole motor simplified model.

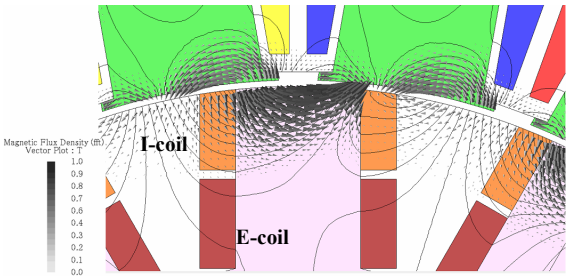

(a) Model 1 (without sub-poles)

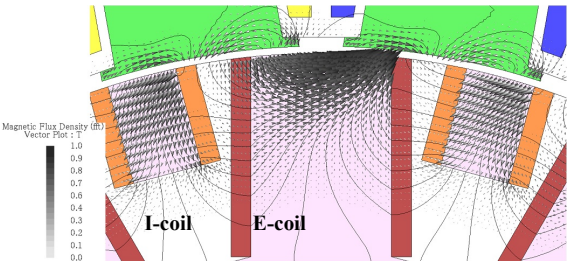

(b) Model 2 (with sub-poles)

Fig. 6. Third space harmonics vector and flux lines.

Figure 6(a) shows a magnetic flux vector and flux lines of the third space harmonics simulated by the magnetic field analysis. As shown in the figure, the third space harmonics magnetic flux mainly flows through a space between the rotor salient poles, of which direction corresponds to the q-axis, and leaks to the salient poles on the d-axis. Therefore, the third space harmonics power can efficiently be retrieved by placing sub-poles on the q-axis as shown in Fig. 6(b). Since Model 1 has both of the induction coil and the excitation coil on the same salient pole, i.e., the d-axis, it is rather difficult to retrieve the third space harmonics power efficiently. Model 2, however, has the induction coil and the excitation coil separately on the q-axis and the d-axis, respectively, which results in effective retrieval of the third space harmonics power.

C. *Effect of Sub-Poles on Torque Characteristics*

Figure 7 shows a cross section diagram of Model 2 that has the I-poles on the q-axis. The I-poles are designed to be

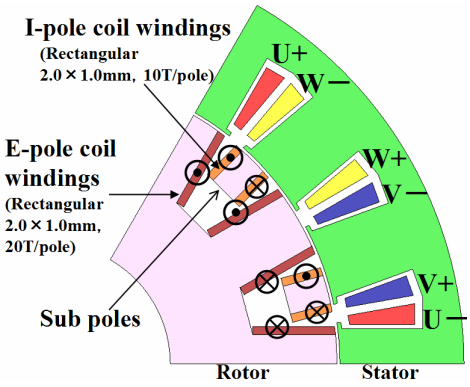

Fig. 9. Cross section diagram of Model 2 (with sub-poles).

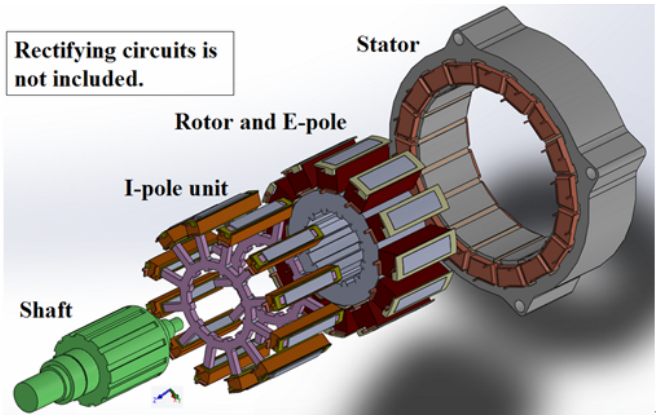

Fig. 10. Mechanical configuration of Model 2.

magnetically independent of a main magnetic flux path to prevent reluctance torque degradation and to concentrate on retrieval of the third space harmonics power. Figure 8 shows a mechanical configuration of the Model 2 motor, where the I-poles are fixed by two endplates from the axial direction.

Figure 9 shows comparison of torque characteristics among the three motors described above at 1000 r/min and 273 A_{pk} under MTPA control calculated by the magnetic field analysis. As shown in the figure, the output torque of Model 2 is improved by 19.5 %, compared with Model 1. Furthermore, the torque ripple of Model 2 is remarkably reduced from that of the normal SynRM. Figure 10 shows an induced current of the series connected I-pole winding in forward direction of the diode rectifying circuit. As can be seen in the figure, the induced current of Model 2 is much higher than that of Model 1, which demonstrates effectiveness of the sub-poles and the separated two windings, i.e., I-pole and E-pole windings. The third space harmonics magnetic flux path is established on the q-axis as expressed in Eq. (10) and illustrated in Fig. 6(b), and the harmonics power can effectively be retrieved by the sub-poles placed on the q-axis, resulting in the higher output torque. The increased induced current of the I-pole winding gives higher field current to the E-pole winding.

The output torque of the proposed motor is expressed as

$$T_{dq} = P_p \left\{ \left(L_d - L_q\right) I_d I_q + M_d(\omega t) I_{rd}(\omega, t) \right\}, \tag{11}$$

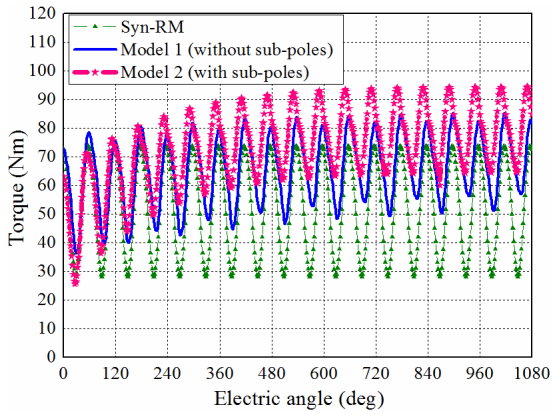

Fig. 7. Torque characteristics at 1000 r/min under MTPA control.

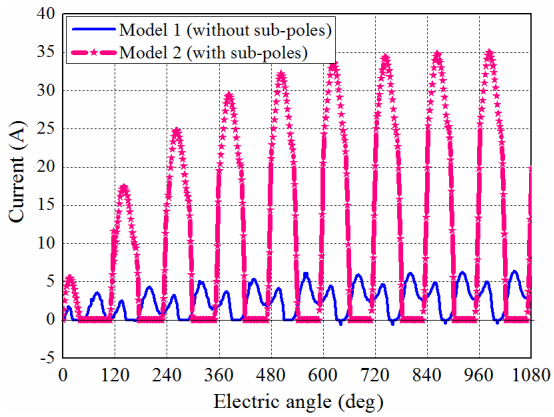

Fig. 8. Induced current waveforms in forward direction.

where P_p is a pole-pair number, L_d and L_q is the d-axis and the q-axis self-inductances, M_d is a mutual inductance between the stator d-axis and the E-pole winding, I_d and I_q are the d-axis and the q-axis armature currents, and I_{rd} is a field current. As expressed in the above equation, the output torque is composed of two terms, i.e., a reluctance torque and a electromagnet torque. The former is basically independent of the operation angular frequency ω. The field current to generate the electromagnet torque, however, is proportional to ω because the q-axis magnetic flux in Eq. (10) links to the I-pole winding and time derivative of Eq. (10) gives an induced voltage in the I-pole winding. In addition, the second term of Eq. (11), i.e., the electromagnet torque, is proportional to the field current of E-pole winding; thus it is essential to feed the current from the I-pole winding.

III. Configuration of Proposed Motor

A. Magnetic Shielding by Minimum Permanent Magnets

The field current of Model 2 is remarkably improved by splitting the rotor winding into I-pole and E-pole windings. However, the torque density of Model 2 in the steady state is still lower than that of the IPM motor. This limitation of the torque density improvement is caused by the fact that only the rotor salient pole produces the electromagnet force in the circumferential direction that contributes torque generation as shown in Fig. 11. On the other hand, the conventional IPM

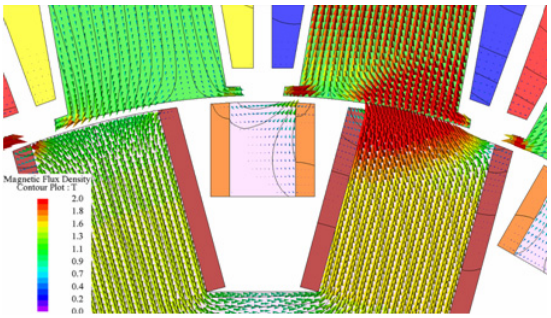

Fig. 11. Magnetic flux vector of Model 2 in CCW rotation.

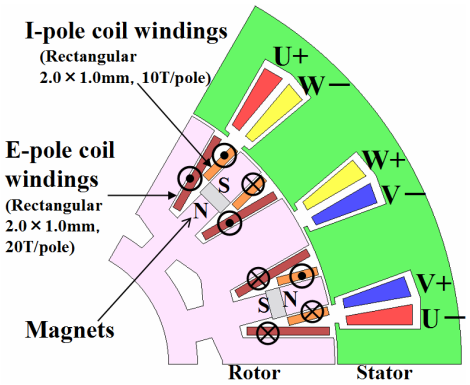

Fig. 12. Cross section diagram of proposed motor.

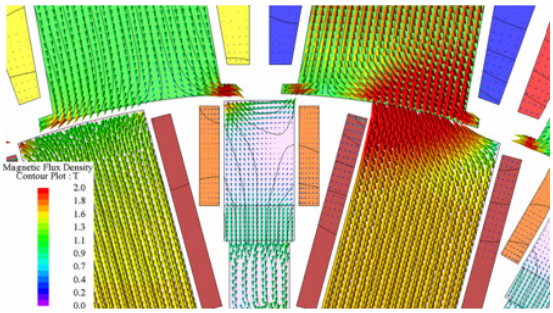

Fig. 13. Magnetic flux vector of proposed motor in CCW rotation.

motor can generate higher electromagnetic force in the circumferential direction by strong armature reaction composed by the armature magnetic flux and the rotor magnets located in the *d*-axis. Therefore, it is possible to generate extra torque with the I-poles without spoiling an inherent I-pole role, i.e., retrieval of the third space harmonics power. This operation can be realized by the armature reaction torque in the I-pole by means of magnetic shielding with small amount of permanent magnets. The armature reaction torque is available by facing the permanent magnet flux toward the armature magnetic flux. Figure 12 shows a configuration of the proposed motor capable to generate the armature reaction torque in the I-poles. Small pieces of the permanent magnets are inserted between the I-poles and the rotor core and its magnetic flux prevent the increase in *d*-axis inductance. In addition, that magnets can generate higher electromagnetic force in the circumferential direction by armature reaction with the same principle of IPM conventional motor. Figure 13 shows a magnetic flux vector when the

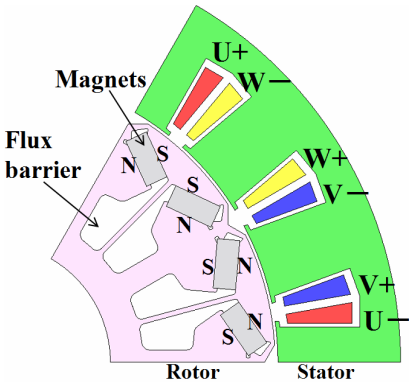

Fig. 14. Cross section diagram of benchmark IPM motor.

proposed motor rotates in the CCW direction. As can be seen in the figure, the armature reaction torque is generated by the I-pole as well as the torque generated by the E-pole.

B. Benchmark IPM Motor

A benchmark IPM motor is designed to compare the torque density with the proposed motor. The IPM motor has a concentrated winding structure in the stator and V-shaped Nd-Fe-B permanent magnets in the rotor as shown in Fig. 14. All of the benchmark, Model 1, Model 2, and the proposed motors are designed on the same basis of the core size and the stator specifications, e.g., iron core materials, gap length and so forth. The only difference among these motors is a magnetic circuit of the rotor. Physical dimensions of one permanent magnet piece are 12 mm by 5.5 mm for the benchmark IPM motor and 7.5 mm by 3.5 mm for the proposed one, respectively. The benchmark is designed to utilize efficiently the reluctance torque as well as the permanent magnet torque by precisely adjusting the magnetic pole opening angle, flux barrier shape and magnet quantity.

IV. Torque Characteristics of Proposed Motor

Figure 15 shows an output torque comparison between the benchmark and the proposed motor. As shown in the figure, the torque density at 1000 r/min of the proposed motor is 8.2 % lower than that of the benchmark, while the proposed motor surpasses the benchmark at 2000 r/min. It can be confirmed that the additional torque generated by the self-excitation using the space harmonics power is significant to satisfy the same level of the total output torque as the benchmark. This additional torque by the I-pole greatly contributes to increase the total output torque regardless of the reduced permanent magnet torque although the permanent magnet volume of the proposed motor is reduced by 81.4 %, compared with the benchmark. Moreover, another superior point of the proposed motor can be found in the torque ripple characteristic. The torque ripple of proposed motor is 18.2 % under MTPA control, which is remarkably improved from Model 2 (43.2 %) and is comparable with the benchmark IPM motor (12.8 %). Figure 16 shows the induced current waveforms. It can be seen that the induced current of proposed motor has a slow falling edge. This waveform improvement reduces the field current ripple and enlarges the E-coil torque. Figure 17 shows current phase-average torque

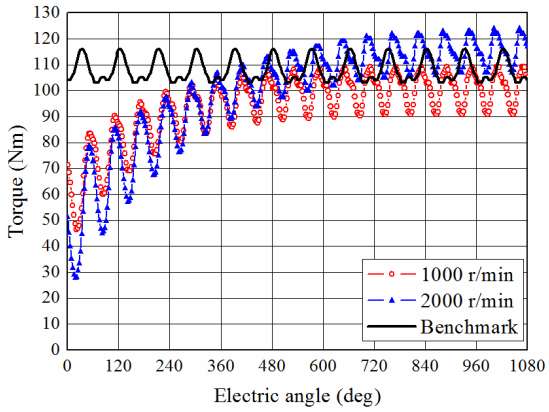

Fig. 15. Torque characteristics of proposed motor.

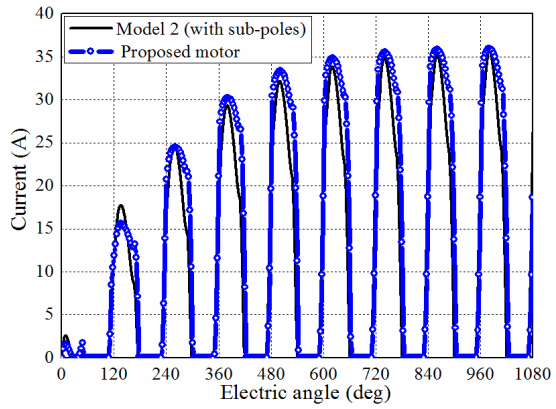

Fig. 16. Induced current characteristics of proposed motor.

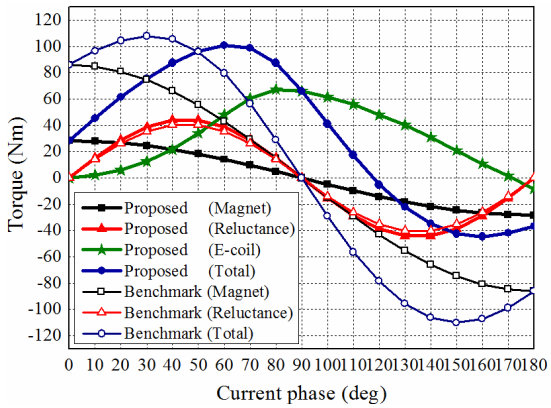

Fig. 17. Current phase-torque characteristics of proposed motor.

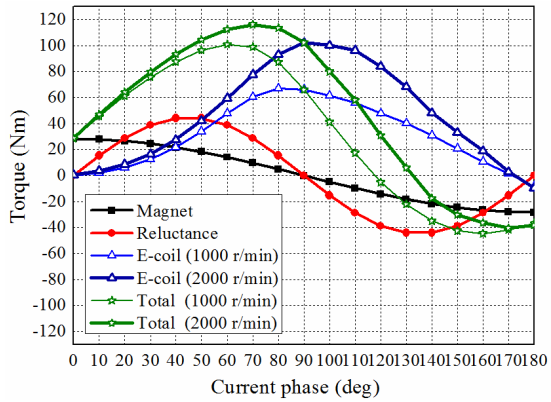

Fig. 18. Current phase-torque characteristics of benchmark and proposed motors.

characteristics of the benchmark and the proposed motors at 1000 r/min. Since the self-excited electromagnet torque has the maximum value at the current phase of 90 deg, the MTPA control point of the proposed motor slightly advances with respect to the current phase, compared with that of the benchmark. Although the magnet torque of the proposed motor is largely decreased due to the small size of the permanent magnet, the total output torque is comparable with the benchmark, owing to the electromagnet torque generated by the E-pole winding. Figure 18 shows adjustable speed drive characteristics of the proposed motor. As indicated by Eq. (11), the electromagnet torque becomes larger as the fundamental synchronous speed rises because the self-excited E-coil torque is proportional to. Also, the MTPA control angle is advanced with increase of ω.

V. CONCLUSION

This paper has proposed a new rare-earth-less motor which can utilize the space harmonics power for the field magnetization. By splitting the rotor winding into the induction pole (I-pole) winding and the excitation pole (E-pole) winding and rectifying the induced current by full-bridge diode rectifier, the space harmonics power can efficiently retrieved and the total output torque can effectively be enhanced. In addition, the output torque characteristic can dramatically be improved by inserting small permanent magnets into the I-poles. The future work is to setup an actual prototype machine and to verify the analysis results through experimental tests.

REFERENCES

[1] M. Azuma, M. Hezeyama, M. Morita, Y. Kuroda, and M. Inoue, "Driving Characteristics of a Claw Pole Motor Using Filed Excitation for Hybrid Electric Vehicles," IEEJ Technical Meeting on Vehicle Technology, pp. 37-40, 2011 (in Japanese).

[2] T. Kosaka, T. Hirose, N. Matsui, and K. Elissa, "Some Considerations on Experimental Drive Characteristics of Less Rare-Earth HEM," IEEJ Transactions on Industry Applications, no.1-O6-2, pp. 85-90, 2011 (in Japanese).

[3] S. Nonaka, "The Self-Excited Type Single-Phase Synchronous Motor," IEEJ Transactions on Industry Applications, vol.78, no. 842, pp. 1430-1438, Nov. 1958 (in Japanese).

[4] S. Nonaka, and K. Akatsu, "Analysis of New Brushless Self-Excited Single-Phase Synchronous Generator by Finite Element Method," IEEJ Transactions on Industry Applications, vol.30, no.3, pp.615-620, 1994.